

1 Application of a spring-dashpot system to clinical lung
2 tumor motion data

3
4 **E J Ackerley¹, A E Cavan^{2,3}, P L Wilson^{1†}, R I Berbeco⁴ and J Meyer^{2,5,‡}**

5
6 ¹Department of Mathematics and Statistics, University of Canterbury, Private Bag 4800,
7 Christchurch 8140, New Zealand

8
9 ²Department of Physics and Astronomy, University of Canterbury, Private Bag 4800,
10 Christchurch 8140, New Zealand

11
12 ³Department of Medical Physics & Bioengineering, Christchurch Hospital, Private Bag 4710,
13 Christchurch, New Zealand

14
15 ⁴Department of Radiation Oncology, Brigham and Women's Hospital, Dana-Farber Cancer
16 Institute and Harvard Medical School, Boston, Massachusetts 02115, USA

17
18 ⁵Department of Radiation Oncology, University of Washington Medical Center, Box 356043,
19 Seattle, Washington 98195-6043, USA

20
21 † Corresponding author: Department of Mathematics and Statistics, University of Canterbury,
22 Private Bag 4800, Christchurch 8140, New Zealand, Phone: +64 3 364 2664, Fax: +64 3
23 364 2587, Email: phillip.wilson@canterbury.ac.nz

24 ‡ Present address: Department of Radiation Oncology, University of Washington, University
25 of Washington Medical Center, 1959 NE Pacific St, Box 356043, Seattle WA 98195

27 **Abstract**

28 A spring-dashpot system based on the Voigt model was developed to model the correlation
29 between abdominal respiratory motion and tumor motion during lung radiotherapy. The
30 model was applied to clinical data comprising 52 treatment beams from 10 patients, treated
31 on the Mitsubishi Real-Time Radiation Therapy system, Sapporo, Japan. In Stage 1, model
32 parameters were optimized for individual patients and beams to determine reference values
33 and to investigate how well the model can describe the data. In Stage 2, for each patient the
34 optimal parameters determined for a single beam were applied to data from other beams to
35 investigate whether a beam-specific set of model parameters is sufficient to model tumor
36 motion over a course of treatment.

37 In Stage 1 the baseline root mean square (RMS) residual error for all individually-optimized
38 beam data was 0.90 ± 0.40 mm. In Stage 2, patient-specific model parameters based on a
39 single beam were found to model the tumor position closely, even for irregular beam data,
40 with a mean increase with respect to Stage 1 values in RMS error of 0.37 mm. On average
41 the obtained model output for the tumor position was 95% of the time within an absolute
42 bound of 2.0 mm and 2.6 mm in Stage 1 and 2, respectively.

43 The model was capable of dealing with baseline, amplitude and frequency variations of the
44 input data, as well as phase shifts between the input tumor and output abdominal signals.
45 These results indicate that it may be feasible to collect patient-specific model parameters
46 during or prior to the first treatment, and then retain these for the rest of the treatment period.
47 The model has potential for clinical application during radiotherapy treatment of lung tumors.

48

49 **Keywords:** spring-dashpot model, radiotherapy, lung tumor modeling, respiration,
50 differential equation

51 **1. Introduction**

52 Lung cancer was the most commonly diagnosed cancer worldwide in 2008, with an
53 incidence rate of over 1.5 million new cases, or 12 % of the total new cancer diagnoses¹. It
54 was also the most common cause of death from cancer, accounting for 17% of all cancer
55 deaths. Radiation therapy is a common modality for lung cancer treatment, however
56 treatment efficacy is limited by the motion of the lungs during respiration², which is primarily
57 driven by diaphragm motion, and to a lesser extent by chest motion. The magnitude of lung
58 tumor motion depends on patient-specific breathing and tumor characteristics, and is usually
59 most pronounced along the superior-inferior (SI) axis, compared to the anterior-posterior
60 (AP) and lateral directions³. One study, which included 39 patients treated with the Real-
61 Time Radiation Therapy system in Sapporo, Japan, found a median tumor movement of 1.1
62 mm, 2.3 mm and 5.4 mm in lateral, AP and SI direction, respectively⁴.

63 Typically, for lung tumors the clinical target volume (CTV) is enlarged to the internal target
64 volume (ITV) with the intent of ensuring sufficient tumor coverage in the presence of motion⁵.
65 This strategy can result in excessive irradiation of surrounding healthy tissue, or marginal
66 miss of the tumor⁶. The high doses required for tumor control are close to or above the
67 tolerance level for healthy tissues, resulting in increased side effects, or requiring a reduction
68 in dose to the tumor, decreasing tumor control probability (TCP)^{7, 8}. In this way,
69 compensating for the presence of respiratory motion of lung tumors can improve the
70 therapeutic ratio and thus survival rates⁹.

71 One means to compensate for tumor motion is by means of real-time tumor tracking and
72 motion compensation^{8, 10-14}. Motion tracking is complicated by variations in baseline,
73 frequency and oscillatory amplitude and form, despite the overall superficial regularity of
74 respiratory motion. These effects can differ widely between patients but can also vary over
75 the course of treatment of a single patient⁷. Methods to suppress such variability include
76 abdominal compression to reduce tumor mobility, breath control techniques (active or

77 passive) and respiratory gating of irradiation^{3, 7, 15-19}, with the latter usually based on external
78 surrogate motion. All of these techniques have some limitations, such as the need for active
79 patient cooperation, consistent ability to maintain total lung capacity²⁰, or a lengthened
80 treatment time for gated therapy due to the required beam-off periods.

81 Modeling of the respiratory-induced lung tumor motion can facilitate dynamic tracking and
82 compensation for real-time and gated treatments^{4, 7, 8, 19}. Direct tumor tracking systems may
83 use portal imaging^{10, 13, 21, 22} or implanted fiducial markers in the tumor, in conjunction with a
84 diagnostic x-ray imaging system^{20, 23, 24}, but this continuous imaging can impart a
85 considerable radiation dose which is not always clinically justifiable²⁵.

86 By contrast, indirect tumor tracking systems use internal or external surrogates to obtain
87 tracking signals. A model is then required to relate the surrogate to tumor motion. Examples
88 of external respiratory surrogates are a spirometer, strain gauge or abdominal markers²⁰,
89 while an internal surrogate can be the diaphragm motion²⁶. Such indirect approaches require
90 the relationship between surrogate and internal tumor motion to be consistent and well
91 correlated²⁷. The benefits of indirect tracking include the elimination of risks associated with
92 changes in the relationship between tumor and implanted marker during radiotherapy⁴,
93 fiducial implantation, extra radiation doses, and direct tracking failures. Most models
94 correlating surrogate data to tumor motion have been so-called 'black box' or 'grey box'
95 approaches, for which the internal behavior of the physical system is not or only partially
96 known, respectively. These models consider the input and output data, but not the exact
97 physical relationship between them. Various approaches of this form include linear
98 correspondence models^{9, 28}, composites of baseline drift, frequency variation, fundamental
99 pattern change and random observation noise⁷, characterization of the motion with a
100 piecewise linear model of defined stages of the breathing cycle²⁹, state-based probabilistic
101 models³⁰, least-squares parameter estimation and systems identification³ or adaptive neural
102 networks³¹. These models generally require a large amount of sample data which
103 encompasses the range of possible relationships between the input and output states. Many

104 of the previous external surrogate models tend to deal poorly with irregularities in the
105 breathing pattern, such as baseline drift or a hysteresis³¹, a lag or phase shift between
106 internal and external motions^{27, 32, 33}, and usually have a strong dependence on tumor and
107 marker locations, motion dimensions and type of breathing pattern^{3, 4, 28}. One of the more
108 promising models is the model by Cervino *et al.*²⁶ using an internal surrogate signal of the
109 diaphragm; however the practical benefits of using an external signal warrant further
110 investigation into external abdominal surrogates.

111 A more physical approach to the problem models lung motion as a contact problem of
112 elasticity theory by describing the physiology of breathing using elastic constants to directly
113 model the lung tissue³⁴. A different approach was explored by Wilson and Meyer^{35, 36} who
114 presented a comprehensive physical 3D system of springs and dashpots to model the
115 correlation of an external abdominal respiratory signal and the lung tumor motion, rather
116 than directly modeling the actual lung tissue²⁴. Wilson and Meyer showed mathematically
117 that it is possible to formally simplify the three-dimensional model to a one-dimensional
118 model when SI motion of the tumor dominates.

119 To overcome some of the physical intrinsic limitations for the practical application of the
120 above approach, the first aim of this paper was to refine the Wilson and Meyer model in the
121 one-dimensional realm. The relationship of lung tumor and external abdominal marker
122 movement is considered for the primary dimension of motion, i.e. the SI and AP direction of
123 the tumor and abdominal signal, respectively. The second objective was to apply the refined
124 model to a large and realistic clinical data set of tumor motion from a cohort of lung cancer
125 patients treated with the Mitsubishi Real-Time Radiation Therapy system in Sapporo, Japan
126 to investigate the model behavior on an intra- and inter-patient specific basis.

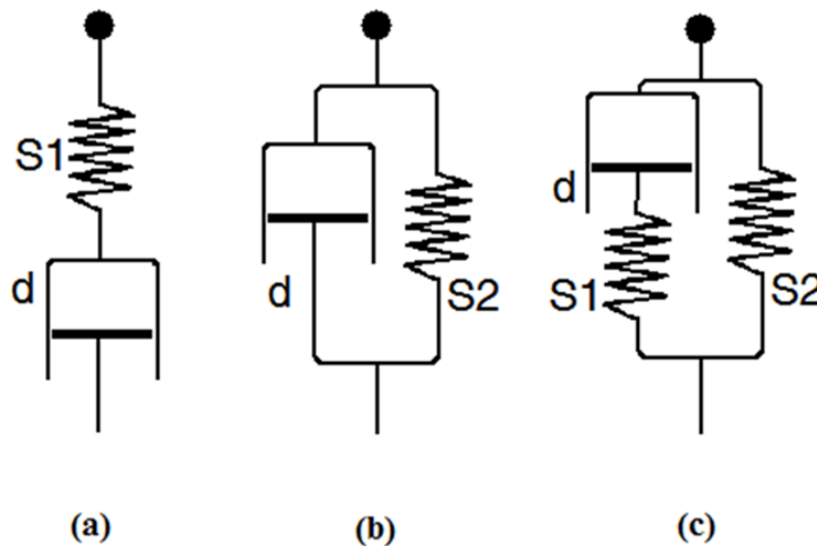
127

128 **2. Material and Methods**

129 *2.1 Mathematical model*

130 Following the methodology of Wilson & Meyer³⁵, we model the correlation between the
 131 surrogate data provided by abdominal motion and the target data of the lung tumor motion
 132 with a pseudo-mechanical system. This system is composed of springs and dashpots, the
 133 latter providing a damping effect. In general, a spring-dashpot unit can be composed of
 134 springs and dashpots in series, parallel, or some combination thereof. Three of the most
 135 frequently-used configurations in other applications are shown in Figure 1. The full three-
 136 dimensional system of Wilson & Meyer (2009) featured a Voigt unit able to act in each
 137 Cartesian direction of motion.¹

138



139

140 **Figure 1:** (a) Maxwell model (b) Voigt model (c) Standard Linear Solid model. S
 141 denotes a spring and *d* denotes a dashpot.

142

143 Asymptotic analysis³⁵ shows that when the SI motion of the tumor is dominant the motion is
 144 well-modeled by a single Voigt unit acting in the SI direction, with the tumor attached at one
 145 end and the abdominal system providing input at the other. It is this pseudo-one dimensional

¹ Note that these were incorrectly drawn in the Wilson & Meyer paper as Maxwell units.

146 class of tumor motion which we consider in this paper. In the following condensed derivation,
147 all variables and parameters are non-dimensional.

148 The variable x is the tumor displacement from a resting equilibrium position in the SI
149 direction. The Hookean spring has associated parameter ω , while the dashpot,
150 characterized by the parameter λ provides a retarding force directly proportional to the tumor
151 velocity. Although the dominant time-dependent abdominal motion, $f(t)$, is in the AP direction
152 perpendicular to the dominant tumor motion direction, this component of the abdominal
153 signal is linearly scaled and used as input to the model. This forcing input signal, $x^*(t)$, is
154 therefore related to the measured data by $x^* = \delta f$, with the scale factor δ being determined
155 under optimization. This approach reduces the dimension of the parameter space of Wilson
156 & Meyer by one, and also allows a wider range of parameter values to be studied, both of
157 which enable the model to be more readily optimized.

158 Following Wilson & Meyer³⁵ but with the above notation, the tumor motion is given by

$$159 \quad \frac{d^2 x}{dt^2} = -2\lambda \frac{dx}{dt} - \omega^2 x + \delta f \quad (1)$$

160 The model will be shown to hold for all patients in this class of tumor motion, with values of
161 the parameter triplet $(\omega, \lambda, \delta)$ derived from a “training” subset of patient data, and
162 successfully applied to model the remaining data.

163

164 *2.2 Numerical approach*

165 Equation (1) was rewritten as two coupled first-order ordinary differential equations, which
166 were solved for each set of training data using the MATLAB™ differential equation solver
167 *ode45*, which is recommended for non-stiff problems³⁷. The resulting output data was
168 optimized with respect to the model parameter triplet $(\omega, \lambda, \delta)$ using the MATLAB
169 *fminsearch* routine in combination with a cost function: an iterative process used to find the

170 minimum of the root mean squared error (RMS) (2) between the measured tumor position
171 data, X , and the model output values, x (at each time step, n).

$$172 \quad RMS = \left(\frac{\sum_{i=1}^n (X - x)^2}{n} \right)^{\frac{1}{2}} \quad (2)$$

173 The algorithm starts with an initial estimate of the triplet based on the model characterization
174 in Wilson & Meyer and proceeds via a process of unconstrained non-linear optimization with
175 a Simplex search method. Optimization is initially patient- and beam-specific and is based on
176 a set of “training” data constituting approximately 2 minutes of patient data. The algorithm
177 terminates when the RMS error is less than 10^{-3} or when a maximum number of 100
178 iterations have been reached.

179 In *Stage 1* of our work, optimized parameters obtained in this way are used to model the
180 tumor motion via numerical solutions to equation (1) for each beam to obtain reference
181 values. We refer to this stage as ‘optimized’.

182 In *Stage 2* (‘non-optimized’) we take the optimized parameters from a single beam – e.g.
183 Day 1, Beam 1– and use these to model the tumor motion via (1) for that patient's
184 respiratory data obtained from other beams on the same day and consecutive days. The
185 comparison between the predicted tumor position, x , and the clinical data, X , is presented
186 and discussed in sections 3 and 4.

187

188 *2.3 Clinical data*

189 The clinical data consists of 3D internal fiducial-based motion obtained using radiopaque
190 fiducial markers implanted and visualized in real-time using stereoscopic diagnostic x-ray
191 fluoroscopy, collected using a Mitsubishi Real-Time Radiation Therapy system, at the
192 Nippon Telegraph and Telephone Corporation Hospital, Sapporo, Japan²⁷. This was

193 obtained simultaneously with 1D external abdominal motion, collected on an independent
194 co-ordinate system using a laser based AZ-733V "RespGate" made by Anzai Medical,
195 Tokyo, Japan. The data set consisted of motion results from eleven patients (patient 1-11)
196 with lung cancer at various sites, with a total of 171 treatment beams for up to ten
197 consecutive treatment fractions (day 1-10) and four beam configurations per fraction (beam
198 1-4)⁽²⁾. The patients were not a random sample of the general lung cancer population, but
199 were selected on the basis of an estimated internal marker motion of more than 10 mm peak
200 to peak (SI, lateral or AP direction). The data show phase shifts of the internal-external data
201 (one signal lagging the other)^{32, 33} in the SI direction that are mostly between 100 and 200
202 ms.

203 The data were not acquired in a common coordinate system with absolute spatial co-
204 ordinates and therefore they could not be normalized to a common reference point. Spatial
205 baselines for the tumor and abdominal markers were defined by normalizing on the mean of
206 each beam data.

207 For baseline values in Stage 1 the model was initially applied to data from 52 treatment
208 beams from 10 patients: beam 1 data for all days for all patients (as this type of data was
209 available for all patients), as well as all beams for patients 1-3. More detailed analysis was
210 then carried out on representative individual patients: one whose model performance was
211 close to the mean of all patients (Patient 7); one with relatively poor model performance
212 (Patient 8); and one with excellent model performance (Patient 10).

213 In the second stage, for each patient the optimal parameters determined for an arbitrarily
214 chosen single beam were applied to data from other beams and treatment days to
215 investigate whether a beam-specific set of model parameters is adequate to model tumor
216 motion over a course of treatment.

⁽²⁾ Patient 5 had eight fractions, then a further four two months later. The analysis was kept consistent. The data for patient 11 were unreliable and not included.

217 We also investigate the ability of the model to adapt to irregularities in the clinical data such
218 as unclear tracking data, missing data points, baseline drift and amplitude and frequency
219 variation.

220

221 **3. Results**

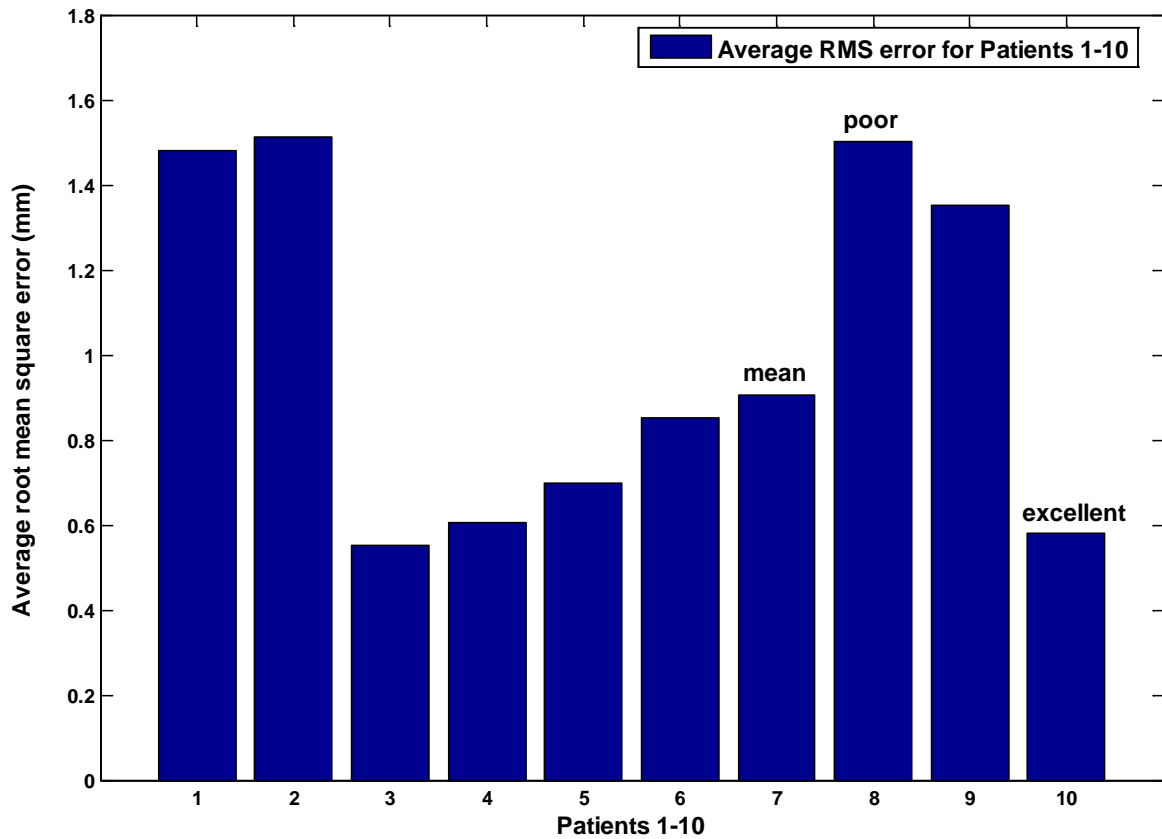
222 *3.1 Stage 1*

223 Applying the optimization algorithm to the data from the 52 clinical treatment beams with the
224 initial estimate parameter triplet $(\omega, \lambda, \delta) = (10, 5, 200)$ gave, on average, a root mean
225 square error of 0.90 mm (2 s.f.) and a standard deviation of 0.40 mm between the modeled
226 position and the tumor motion in the superior-inferior direction. The best result from all the
227 beam data modeled, Patient 4, Day 1, Beam 1, had an RMS error of 0.38 mm. An overview
228 of the RMS errors for all patients is shown in Figure 2.

229 The number of iterations required for optimization varied considerably with each beam but
230 was generally less than 100 iterations. A representative example (patient 7) of beam data
231 and the model results with a RMS of 0.69 mm is shown in Figure 3, with optimized
232 parameters $\omega = 10.12$, $\lambda = 5.27$, $\delta = 197.91$.

233 The linear relationship between the position predicted by the model and the actual tumor
234 location was investigated, and the regression correlation coefficient was calculated for each
235 beam studied. The mean correlation from all 52 beams was 0.96 with standard deviation of
236 0.03, which would indicate the existence of strong linear relationships. A graphical analysis
237 of one beam each for the three representative patients is shown in the top row of Figure 4.

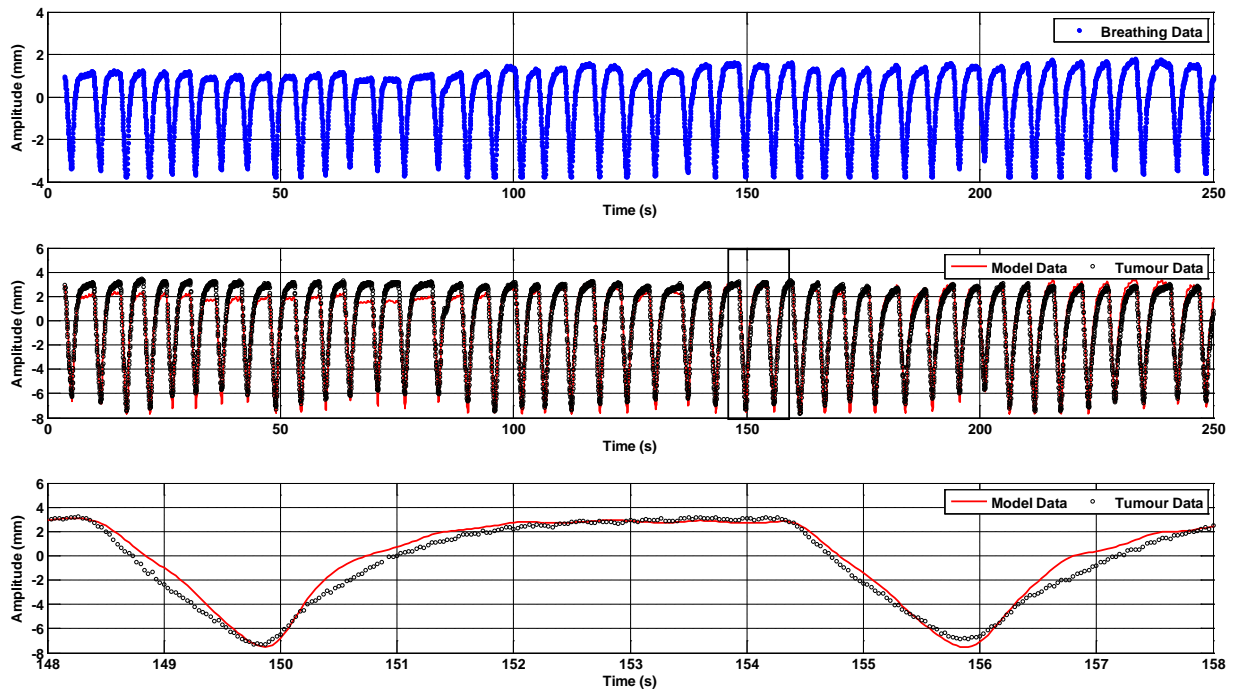
238



239

240 **Figure 2:** Average root mean square error (mm) between model output and clinical data for
 241 each patient. Representative patients 7, 8 and 10 used for further analysis are marked as
 242 'mean', 'poor' and 'excellent', respectively. Note that the number of beams included to
 243 calculate the RMS errors varies between patients.

244



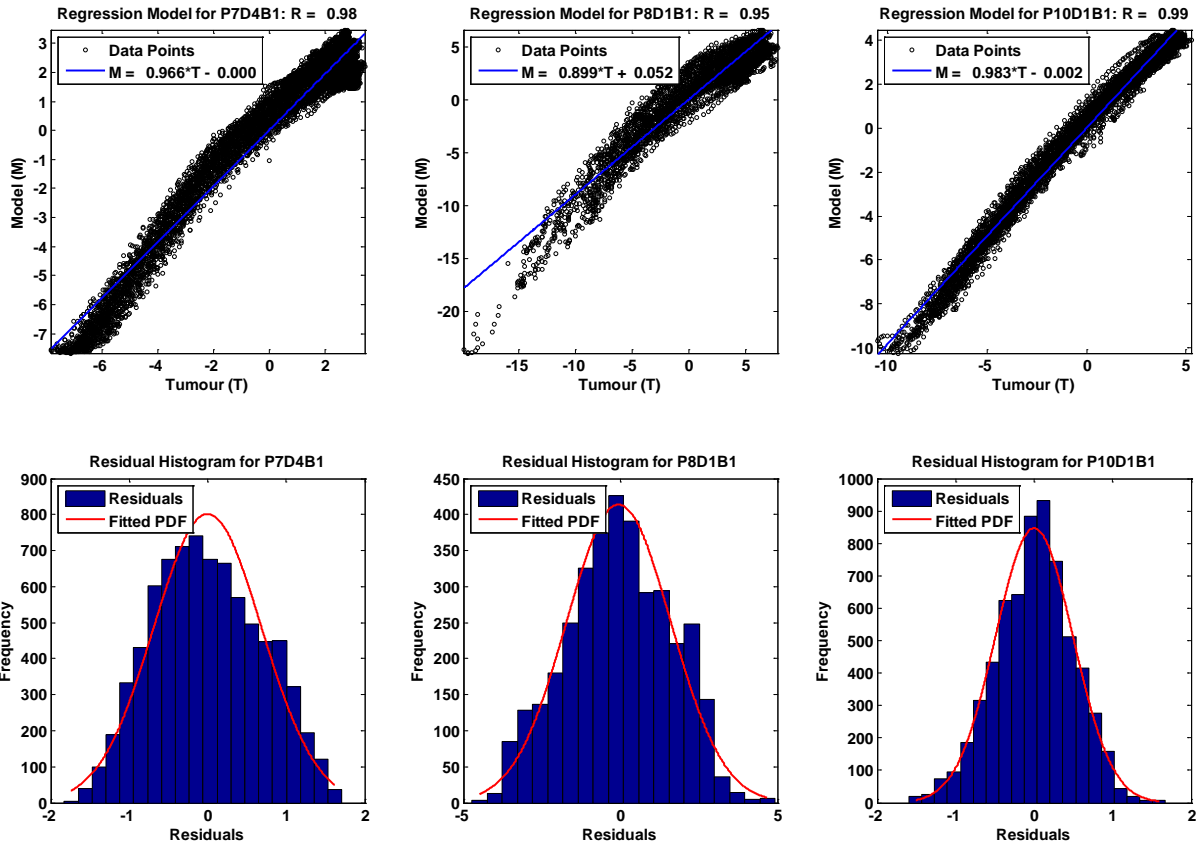
245

246 **Figure 3:** The clinical data and model output, showing breathing pattern, tumor motion, and
 247 model output for Patient 7, Day 4, Beam 1. The lower figure shows a close-up view of part of
 248 the tumor data and model output.

249

250 Additionally, we considered the residual vectors for each beam, which appeared visually to
 251 have a normal-like distribution, although a more rigorous testing of these vectors revealed
 252 that only four beams were sufficiently normal to satisfy the Jarque-Bera³⁸ test. The bottom
 253 row of Figure 4 shows the histograms of three beams. Note that the best fitting probability
 254 distribution is scaled to the area of the histograms. The full width at half maximum was 1.6
 255 mm, 3.9 mm and 1.2 mm for patients 7, 8 and 10, (mean, poor, excellent), respectively.

256



257

258 **Figure 4:** Regression plots and residual histograms for three beams: “mean” Patient 7, Day
 259 4, Beam 1 (left); “poor” Patient 8, Day 1, Beam 1 (center); “excellent” Patient 10, Day 1,
 260 Beam 1 (right).

261

262 For clinical applications, a major concern is the proportion of time, which we term the
 263 *residency*, for which the model output is within a small distance of the actual tumor position,
 264 i.e. within the treatment margin. The residency of the 52 beams was calculated for bounds
 265 on the absolute difference in positions of 1, 2, 3, 4, 5 mm. The residencies from Patients 7, 8
 266 and 10, and all 52 beams are shown in Table 1. As can be seen from the table, to be
 267 resident 95% of the time a bound of 2 mm is required on average. In the second stage the
 268 parameter results obtained from optimizing the Day 1, Beam 1 data for each patient were
 269 applied to other beams and days for that patient in lieu of optimizing the data from each

270 beam independently (Stage 1). There was an average increase in RMS error of 0.37 mm.

271 Results are shown in Table 2.

272 When the robustness of the model was examined with respect to the linear relationship

273 between the tumor position and model prediction, the mean correlation coefficient of the 52

274 beams was 0.96, the same value as when each beam was optimized independently.

275 There was a drop in residency in this second stage as can be seen from Table 3. This time a

276 band width of 2.6 mm was required on average, an increase of 0.60 mm, for 95% residency.

277

278 **Table 1:** Residency analysis for Patient 7, Patient 8, Patient 10 and all 52 beams studied

279 (Stage 1).

Band Width	1 mm	2 mm	3 mm	4 mm	5 mm
Patient 7	72%	97%	99%	100%	100%
Patient 8	50%	84%	96%	99%	99%
Patient 10	92%	99%	100%	100%	100%
All 52 beams	76%	95%	99%	100%	100%

280

281 **Table 2:** Comparison of RMS error results for Patient 7, Patient 8, Patient 10 and all 52
 282 beams studied.

	Average RMS error		
	Stage 1: optimized	Stage 2: non-optimized	Difference
Patient 7	0.91 mm	1.16 mm	0.25 mm
Patient 8	1.50 mm	1.70 mm	0.20 mm
Patient 10	0.58 mm	0.70 mm	0.12 mm
All 52 beams	0.90 mm	1.27 mm	0.37 mm

283

284 **Table 3:** Residency analysis for Patient 7, Patient 8, Patient 10 and all 52 beams without
 285 further optimization (i.e. Stage 2), using Day 1, Beam 1 parameters.

286

Band Width	1 mm	2 mm	3 mm	4 mm	5 mm
Patient 7	62%	91%	99%	100%	100%
Patient 8	42%	77%	94%	99%	99%
Patient 10	85%	99%	100%	100%	100%
All 52 beams	56%	88%	98%	99%	100%

287

288 *3.1.1 Detailed analysis of Patients 7, 8, and 10*

289 The means in Table 2 for patients 7, 8, and 10 were obtained from a subset of data available
 290 for those patients. Now we consider all available and reliable data for patients 7, 8, and 10 to
 291 determine whether our initial use of a subset of data biased the results shown in Table 2. In

292 Table 4 we show that no such bias exists, because when all available and reliable³ beam
 293 data for Patient 7, Patient 8 and Patient 10 were analyzed, the RMS error and residency
 294 results for Patients 7 and 8 calculated from optimized results from all available beam data
 295 are close to the values shown in Table 2. The changes in the mean correlation coefficients
 296 for Patients 7 and 8 were negligible (about 0.96 in all cases) whereas the mean correlation
 297 coefficient for Patient 10 dropped from 0.99 to 0.98 when all available beam data were
 298 analyzed, in both Stage 1 and Stage 2.

299

300 **Table 4:** Comparison results for all available and reliable data for Patient 7, Patient 8,
 301 Patient 10, and all 52 beams studied.

	Average RMS error		Band width for 95% residency	
	Stage 1 optimized	Stage 2 non-optimized	Stage 1 optimized	Stage 2 non-optimized
Patient 7	0.95 mm	1.36 mm	2.1 mm	2.9 mm
Patient 8	1.61 mm	1.87 mm	3.0 mm	3.5 mm
Patient 10	0.84 mm	0.95 mm	1.7 mm	2.0 mm
All 52 beams	0.90 mm	1.27 mm	2.0 mm	2.6 mm

302

³One beam was omitted for patient 10 because it contained a substantial amount of missing data, and obviously spurious measurements.

303 *3.1.2 Sensitivity of optimization for different days.*

304 To test the sensitivity to beam and day parameter optimization, non-optimized results were
305 obtained for Patients 7, 8, and 10 using the parameters obtained from optimizing the Day 3,
306 Beam 2 data, a choice made arbitrarily. The change in the average RMS error and the band
307 width required for 95% residency was small as can be seen from Table 5 below, and there
308 was no change in the mean correlation results. This would indicate that different parameter
309 sets obtained from different beams for the same patient give adequate results.

310

311 **Table 5:** Results for all available and reliable data for Patient 7, Patient 8, and Patient 10
312 optimized using Day 3, Beam 2 parameters.

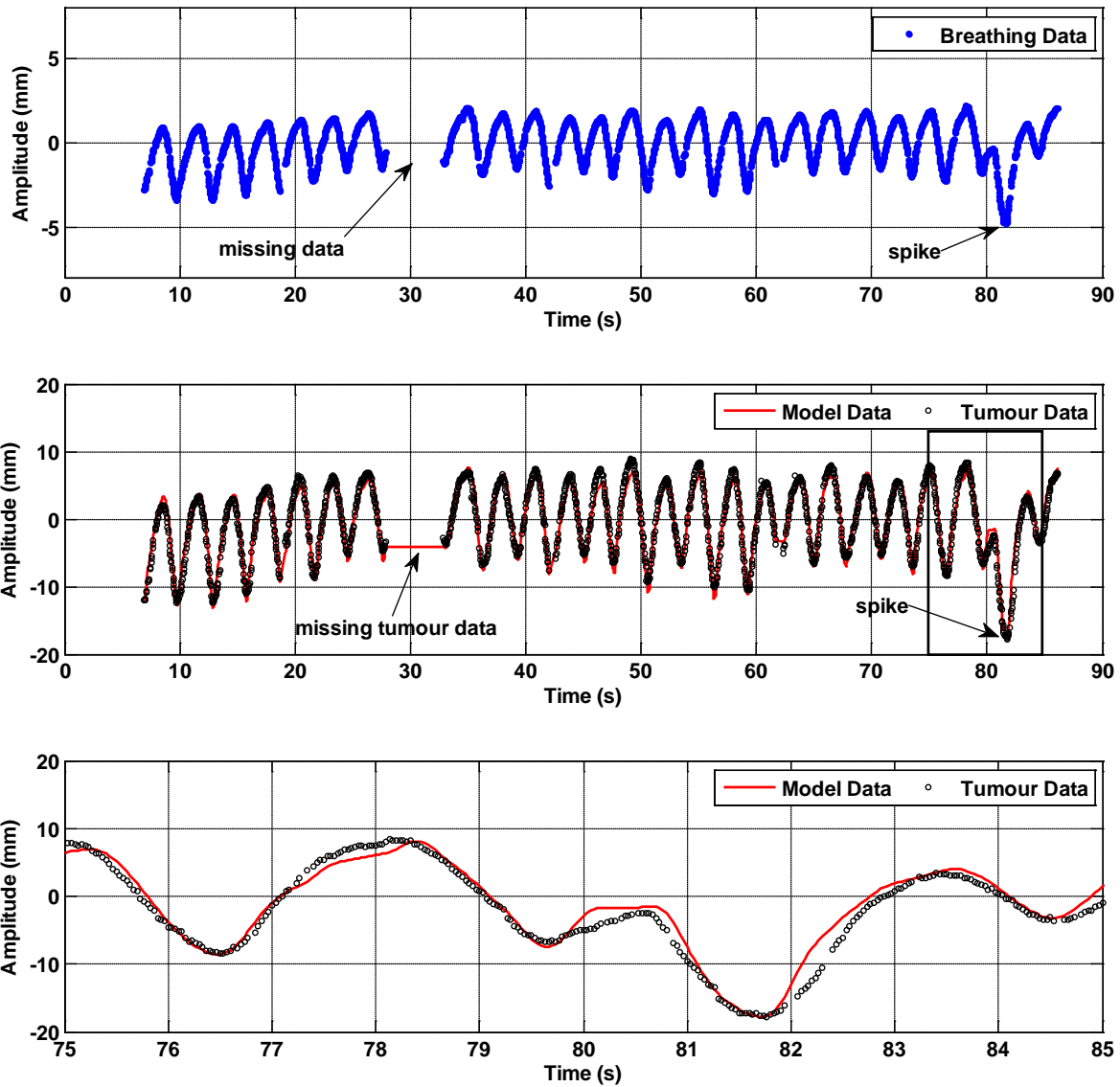
	Average RMS error	Mean correlation coefficient	Band width for 95% residency
Patient 7	1.17 mm	0.96	2.5 mm
Patient 8	1.91 mm	0.96	3.6 mm
Patient 10	0.95 mm	0.98	2.0 mm

313

314 *3.4 Irregular beam data*

315 The model was capable of dealing with data containing irregularities such as missing data
316 covering several seconds (poor tracking of the abdominal motion), spikes in the amplitude of
317 tumor motion and baseline drift. Figure 5 shows an example of the model applied to data
318 containing some initial baseline drift of the breathing signal, a period of missing data, and an
319 unusual rapid variation in amplitude, or "spike". These data problems are important
320 considerations for modeling lung tumor motion to ensure that errors are not avoidably high.

321



322

323 **Figure 5:** Breathing data (top) and tumor data and model output (middle) for Patient 8, Day
 324 2, Beam 1. Labeled are a lengthy period of missing data and a "spike" in the data. The solid
 325 line for the model data is an interpolation between points and therefore does not represent
 326 actual model output; specifically, the model makes no predictions during periods of missing
 327 breathing data. An initial baseline drift is also apparent. The lower figure shows in greater
 328 resolution how the model copes with the data spike.

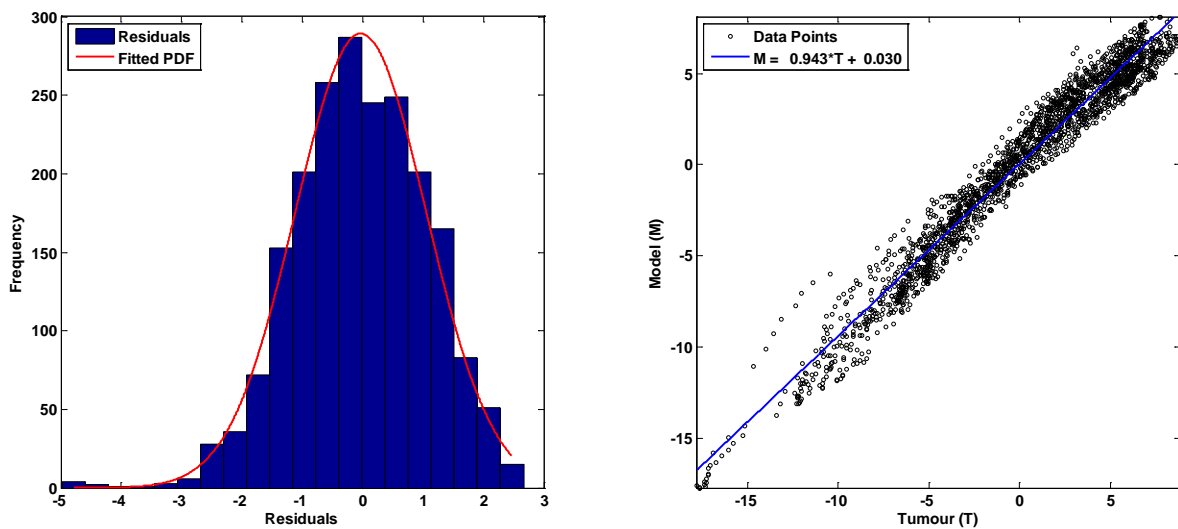
329

330 This incomplete data gives a useful clarification of the functioning of the model. The model
 331 was not designed to predict tumor motion in the absence of breathing data, only in the
 332 absence of tumor data. Thus we see that when the breathing data is missing the model

333 makes no prediction for tumor location. This can be clearly seen in the long period of missing
334 data around 30s, and also in the much shorter periods around 19s and 62s. In all cases, we
335 have plotted an interpolated solid line for the model data for consistency with other plots,
336 although in actual fact the model makes no prediction at those times of missing breathing
337 data.

338

339 The RMS error for this beam data is 1.09 mm and the correlation coefficient is 0.98. The
340 band width for 95% residency is 2.1 mm. These results indicate that the model deals well
341 with irregularities in the data. Figure 6 below shows the histogram of residuals and the
342 regression plot for the data presented in Figure 5. The tail of negative residuals in this
343 histogram is long relative to those shown in Figure 4. This is not due to poor systematic
344 performance but rather due to the performance in the short recovery period immediately
345 following the spike in Figure 5, lasting less than one second.



346

347

348 **Figure 6:** Residual plot (left) and regression plot (right) for Patient 8, Day 2, Beam 1. The

349 mean is -0.030 and standard deviation 1.09, while the correlation coefficient is 0.98.

350

351 **4. Discussion**

352 A modified version of the Wilson & Meyer spring-dashpot model has been developed to
353 correlate abdominal motion with lung tumor motion. In its current implementation the
354 approach is capable of modeling the main component of tumor motion in the SI direction.
355 The model was applied to clinical tumor tracking data from 10 patients treated on the
356 Mitsubishi Real-Time Radiation Therapy system in Sapporo, Japan. In the first stage, the
357 model parameters were optimized for each individual beam in order to determine the
358 goodness of fit for each data set. These values served as a benchmark for further evaluation
359 in Stage 2. In Stage 2, the optimized model parameters for one particular beam were used to
360 estimate the output, i.e. tumor motion, for other beams and treatment days in order to
361 evaluate the trade-offs with regard to optimizing each individual beam separately. The
362 motivation for this was to find out whether it is possible for model parameters to be
363 determined on the first day of treatment or even prior to treatment. The average error
364 determined for Stage 1 was 0.90 ± 0.40 mm, which increased by 0.37 mm in Stage 2. The
365 results were very similar if parameters were used that were initially estimated for other
366 beams for the same patient. This indicates that despite the temporal changes in the
367 abdominal/tumor motion relationship over a treatment course the physical characteristics
368 remain fairly constant, which is reflected in only a small increase in the residual error. This is
369 the advantage of a semi-physical model, such as the one presented here, which aims to
370 model the tissue elasticity as opposed other models which might provide an excellent fit to
371 the input/output data but have no intrinsic relationship to the actual mechanical tissue
372 properties.

373 To put the results into a more clinically relevant context, hypothetical bounds were calculated
374 so that the modeled point location of the tumor would be within the actual point location of
375 the tumor for 95% of the treatment time. This hypothetical bound would account for the
376 inaccuracies of the modeling and assumes otherwise perfect compensation of the tumor
377 motion, by tumor tracking or respiratory gating, for example. The bound calculated for stage

378 1 averaged over 52 beams was 2.0 mm and for Stage 2 it was 2.6 mm. To obtain a better
379 understanding of the variability within the patients, three representative patients were further
380 analyzed, patients 7, 8 and 10, corresponding to a residual error of 0.95 mm ('mean'), 1.61
381 mm (poor') and 0.84 mm ('excellent') in Stage 1. The residual errors showed a largely
382 Gaussian distribution with minimal offset from the mean indicating that the model did not
383 result in systematic model output errors. The calculated error bounds based on the 95%
384 inclusion criteria calculated for the selected patients were 2.1, 3.0, 1.7 mm, respectively,
385 which gives an indication of the correlation between the residual modeling errors and the
386 resulting position uncertainty, which ultimately feeds into the calculation of appropriate
387 margins.

388 One of the useful features of the spring-dashpot system is that it managed to successfully
389 model baseline drifts and irregular tumor motion. It was also capable of quickly restoring
390 accurate model output when data was missing as shown in Figure 5. The determination of
391 optimal modeling parameters did not include a systematic search of the global parameter
392 space; a downhill search algorithm was used for efficiency. It remains to be investigated if a
393 stochastic search technique, e.g. simulated annealing or approximate Bayesian
394 computation, is required to remove dependence on the initial parameter estimates, but this
395 will be at the expense of higher computational costs. For consistency the initial starting
396 condition for the search was kept constant but it was found that the nominal values of the
397 optimized parameters diverged if different starting conditions were used (data not shown).
398 However, it was found that the resulting residuals were almost identical, which indicates that
399 the solution space is relatively flat. Therefore it was not considered critical but remains an
400 area of further investigation.

401 For clinical implementation, several extensions to the current modeling process are needed.
402 One is the extension to a full three dimensional system which also considers the minor axes
403 of tumor motion (AP and lateral) for the sake of completeness for the proportion of patients
404 where this motion is non-negligible. Also, ideally the system should be predictive, as there is

405 a finite time required for the treatment machinery (couch⁸ or multi-leaf collimator¹²) to adjust
406 to the determined change in position. Ultimately, any algorithm has limitations and is
407 dependent on the quality of the input data and therefore the output of the model should be
408 tested and verified with independent means in a clinical setting.

409

410 **5. Conclusion**

411 A semi-physical spring-dashpot model to correlate breathing to tumor motion in the superior-
412 inferior direction has been presented and applied to clinical tracking data. Optimized model
413 parameters were found to be robust and transferrable to different beams on the same day
414 and consecutive days. Day-to-day variations in the agreement between the model output
415 and the measured data were small, indicating that the model parameters may be determined
416 prior to or on the first day of treatment and then used throughout the course of treatment.
417 The semi-physical nature of the model enabled it to deal with irregularities in the data such
418 as baseline drifts, phase shifts and amplitude and frequency variations. Further work will
419 address the expansion of the model to include all three dimensions and experimental testing
420 and verification of the model output in a clinical setting.

421

422 **Acknowledgements**

423 We would like to thank Dr. Seiko Nishioka and Dr. Hiroki Shirato, for the clinical data
424 provided from the Nippon Telegraph and Telephone Corporation Hospital in Sapporo, Japan.
425 Thanks also to the Canterbury Medical Research Foundation for financial support for Alicia
426 Cavan.

427

428 **References**

- 429 1. D. M. Parkin, F. Bray, J. Ferlay and P. Pisani, "Global cancer statistics, 2002," CA: a
430 cancer journal for clinicians **55**, 74-108 (2005).
- 431 2. T. Bortfeld, S. B. Jiang and E. Rietzel, "Effects of motion on the total dose
432 distribution," Semin Radiat Oncol **14**, 41-51 (2004).
- 433 3. J. Meyer, K. Baier, J. Wilbert, M. Guckenberger, A. Richter and M. Flentje, "Three-
434 dimensional spatial modelling of the correlation between abdominal motion and lung
435 tumour motion with breathing," Acta Oncologica **45**, 923-934 (2006).
- 436 4. R. Onimaru, H. Shirato, M. Fujino, K. Suzuki, K. Yamazaki, M. Nishimura, H. Dosaka-
437 Akita and K. Miyasaka, "The effect of tumor location and respiratory function on
438 tumor movement estimated by real-time tracking radiotherapy (RTRT) system," Int J
439 Radiat Oncol Biol Phys **63**, 164-169 (2005).
- 440 5. ICRU62, Report No. ICRU Report 62, 1999.
- 441 6. A. M. Allen, K. M. Siracuse, J. A. Hayman and J. M. Balter, "Evaluation of the
442 influence of breathing on the movement and modeling of lung tumors," Int J Radiat
443 Oncol Biol Phys **58**, 1251-1257 (2004).
- 444 7. D. Ruan, J. A. Fessler, J. M. Balter and P. J. Keall, "Real-time profiling of respiratory
445 motion: baseline drift, frequency variation and fundamental pattern change," Phys
446 Med Biol **54**, 4777-4792 (2009).
- 447 8. J. Wilbert, J. Meyer, K. Baier, M. Guckenberger, C. Herrmann, R. Heß, C. Janka, L.
448 Ma, T. Mersebach, A. Richter, M. Roth, K. Schilling and M. Flentje, "Tumor tracking
449 and motion compensation with an Adaptive Tumor Tracking System (ATTS): System
450 description and prototype testing," Medical Physics **35**, 3911-3921 (2008).
- 451 9. E. Nioutsikou, Y. Seppenwoolde, J. R. Symonds-Tayler, B. Heijmen, P. Evans and S.
452 Webb, "Dosimetric investigation of lung tumor motion compensation with a robotic
453 respiratory tracking system: an experimental study," Med Phys **35**, 1232-1240
454 (2008).

- 455 10. J. Meyer, A. Richter, K. Baier, J. Wilbert, M. Guckenberger and M. Flentje, "Tracking
456 moving objects with megavoltage portal imaging: A feasibility study," *Medical Physics*
457 **33**, 1275-1280 (2006).
- 458 11. M. J. Murphy, "Tracking moving organs in real time," *Semin Radiat Oncol* **14**, 91-100
459 (2004).
- 460 12. P. J. Keall, H. Cattell, D. Pokhrel, S. Dieterich, K. H. Wong, M. J. Murphy, S. S.
461 Vedam, K. Wijesooriya and R. Mohan, "Geometric accuracy of a real-time target
462 tracking system with dynamic multileaf collimator tracking system," *Int J Radiat Oncol*
463 *Biol Phys* **65**, 1579-1584 (2006).
- 464 13. J. Rottmann, M. Aristophanous, A. Chen, L. Court and R. Berbeco, "A multi-region
465 algorithm for markerless beam's-eye view lung tumor tracking," *Phys Med Biol* **55**,
466 5585-5598 (2010).
- 467 14. R. I. Berbeco, F. Hacker, D. Ionascu and H. J. Mamon, "Clinical feasibility of using an
468 EPID in CINE mode for image-guided verification of stereotactic body radiotherapy,"
469 *Int J Radiat Oncol Biol Phys* **69**, 258-266 (2007).
- 470 15. D. Ruan, J. A. Fessler, J. M. Balter, R. I. Berbeco, S. Nishioka and H. Shirato,
471 "Inference of hysteretic respiratory tumor motion from external surrogates: a state
472 augmentation approach," *Phys Med Biol* **53**, 2923-2936 (2008).
- 473 16. M. Partridge, A. Tree, J. Brock, H. McNair, E. Fernandez, N. Panakis and M. Brada,
474 "Improvement in tumour control probability with active breathing control and dose
475 escalation: a modelling study," *Radiother Oncol* **91**, 325-329 (2009).
- 476 17. K. E. Rosenzweig, J. Hanley, D. Mah, G. Mageras, M. Hunt, S. Toner, C. Burman, C.
477 C. Ling, B. Mychalczak, Z. Fuks and S. A. Leibel, "The deep inspiration breath-hold
478 technique in the treatment of inoperable non-small-cell lung cancer," *Int J Radiat*
479 *Oncol Biol Phys* **48**, 81-87 (2000).
- 480 18. S. Shimizu, H. Shirato, S. Ogura, H. Akita-Dosaka, K. Kitamura, T. Nishioka, K.
481 Kagei, M. Nishimura and K. Miyasaka, "Detection of lung tumor movement in real-
482 time tumor-tracking radiotherapy," *Int J Radiat Oncol* **51**, 304-310 (2001).

- 483 19. I. Land, J. A. Mills, K. Young, O. Haas and A. Wilson, "Modelling the effects of lung
484 tumour motion on planning and dose delivery with gated radiotherapy," *Clin Oncol (R
485 Coll Radiol)* **19**, S36 (2007).
- 486 20. H. Yan, F. F. Yin, G. P. Zhu, M. Ajlouni and J. H. Kim, "The correlation evaluation of
487 a tumor tracking system using multiple external markers," *Med Phys* **33**, 4073-4084
488 (2006).
- 489 21. K. Baier and J. Meyer, "Fast image acquisition and processing on a TV camera-
490 based portal imaging system," *Z. Med. Phys.* **15**, 1-4 (2005).
- 491 22. R. I. Berbeco, H. Mostafavi, G. C. Sharp and S. B. Jiang, "Towards fluoroscopic
492 respiratory gating for lung tumours without radiopaque markers," *Phys Med Biol* **50**,
493 4481-4490 (2005).
- 494 23. R. I. Berbeco, S. B. Jiang, G. C. Sharp, G. T. Chen, H. Mostafavi and H. Shirato,
495 "Integrated radiotherapy imaging system (IRIS): design considerations of tumour
496 tracking with linac gantry-mounted diagnostic x-ray systems with flat-panel
497 detectors," *Phys Med Biol* **49**, 243-255 (2004).
- 498 24. H. Shirato, S. Shimizu, T. Kunieda, K. Kitamura, M. van Herk, K. Kagei, T. Nishioka,
499 S. Hashimoto, K. Fujita, H. Aoyama, K. Tsuchiya, K. Kudo and K. Miyasaka,
500 "Physical aspects of a real-time tumor-tracking system for gated radiotherapy," *Int J
501 Radiat Oncol Biol Phys* **48**, 1187-1195 (2000).
- 502 25. Q. Ren, S. Nishioka, H. Shirato and R. I. Berbeco, "Adaptive prediction of respiratory
503 motion for motion compensation radiotherapy," *Phys Med Biol* **52**, 6651-6661 (2007).
- 504 26. L. I. Cervino, A. K. Chao, A. Sandhu and S. B. Jiang, "The diaphragm as an
505 anatomic surrogate for lung tumor motion," *Phys Med Biol* **54**, 3529-3541 (2009).
- 506 27. D. Ionascu, S. B. Jiang, S. Nishioka, H. Shirato and R. I. Berbeco, "Internal-external
507 correlation investigations of respiratory induced motion of lung tumors," *Med Phys*
508 **34**, 3893-3903 (2007).
- 509 28. E. Kanoulas, J. A. Aslam, G. C. Sharp, R. I. Berbeco, S. Nishioka, H. Shirato and S.
510 B. Jiang, "Derivation of the tumor position from external respiratory surrogates with

- 511 periodical updating of the internal/external correlation," *Phys Med Biol* **52**, 5443-5456
512 (2007).
- 513 29. H. Wu, G. Sandison, L. Zhao, Q. Zhao, H. Shirato and S. Jiang, "Correlation between
514 parameters describing tumour motion and its location in the lungs," *Australas Phys
515 Eng Sci Med* **30**, 341-344 (2007).
- 516 30. A. Kalet, G. Sandison, H. Wu and R. Schmitz, "A state-based probabilistic model for
517 tumor respiratory motion prediction," *Phys Med Biol* **55**, 7615-7631 (2010).
- 518 31. M. Isaksson, J. Jalden and M. J. Murphy, "On using an adaptive neural network to
519 predict lung tumor motion during respiration for radiotherapy applications," *Med Phys*
520 **32**, 3801-3809 (2005).
- 521 32. J. D. Hoisak, K. E. Sixel, R. Tirona, P. C. Cheung and J. P. Pignol, "Correlation of
522 lung tumor motion with external surrogate indicators of respiration," *Int J Radiat
523 Oncol Biol Phys* **60**, 1298-1306 (2004).
- 524 33. P. C. Chi, P. Balter, D. Luo, R. Mohan and T. Pan, "Relation of external surface to
525 internal tumor motion studied with cine CT," *Med Phys* **33**, 3116-3123 (2006).
- 526 34. R. Werner, J. Ehrhardt, R. Schmidt and H. Handels, "Patient-specific finite element
527 modeling of respiratory lung motion using 4D CT image data," *Med Phys* **36**, 1500-
528 1511 (2009).
- 529 35. P. L. Wilson and J. Meyer, "A spring-dashpot system for modelling lung tumour
530 motion in radiotherapy," *Computational and Mathematical Methods in Medicine* **11**,
531 13-26 (2010).
- 532 36. P. L. Wilson and J. Meyer, "A General Model of Lung Tumour Motion," in *Progress in
533 Industrial Mathematics at ECMI 2008, Vol. 15*, edited by A. D. Fitt, J. Norbury, H.
534 Ockendon and E. Wilson (Springer Berlin Heidelberg, 2010), pp. 1061-1066.
- 535 37. J. C. Lagarias, J. A. Reeds, M. H. Wright and P. E. Wright, "Convergence Properties
536 of the Nelder-Mead Simplex Method in Low Dimensions," *SIAM Journal of
537 Optimization* **9**, 112-147 (1998).

538 38. C. M. Jarque and A. K. Bera, "A Test for Normality of Observations and Regression
539 Residuals," *Int Stat Rev* **55**, 163-172 (1987).

540

541